Rock Mech Rock Eng (2017) 50:1753–1765
DOI 10.1007/s00603-017-1203-5

ORIGINAL PAPER

Mechanical Properties of Gas Shale During Drilling Operations

Chuanliang Yan[1,2] · Jingen Deng[2] · Yuanfang Cheng[1] · Menglai Li[3] · Yongcun Feng[4] · Xiaorong Li[4]

Received: 27 March 2016 / Accepted: 12 March 2017 / Published online: 18 March 2017

Abstract The mechanical properties of gas shale significantly affect the designs of drilling, completion, and hydraulic fracturing treatments. In this paper, the microstructure characteristics of gas shale from southern China containing up to 45.1% clay were analyzed using a scanning electron microscope. The gas shale samples feature strongly anisotropic characteristics and well-developed bedding planes. Their strength is controlled by the strength of both the matrix and the bedding planes. Conventional triaxial tests and direct shear tests are further used to study the chemical effects of drilling fluids on the strength of shale matrix and bedding planes, respectively. The results show that the drilling fluid has a much larger impact on the strength of the bedding plane than that of the shale matrix. The impact of water-based mud (WBM) is much larger compared with oil-based mud. Furthermore, the borehole collapse pressure of shale gas wells considering the effects of drilling fluids are analyzed. The results show that the collapse pressure increases gradually with the increase of drilling time, especially for WBM.

✉ Chuanliang Yan
yanchuanliang@163.com

✉ Yongcun Feng
yongcun.f@gmail.com

[1] School of Petroleum Engineering, China University of Petroleum (East China), Qingdao, China

[2] State Key Laboratory of Petroleum Resource and Prospecting, China University of Petroleum (Beijing), Beijing, China

[3] Key Laboratory of Shale Gas Exploration, Ministry of Land and Resources, Chongqing Institute of Geology and Mineral Resources, Chongqing, China

[4] The University of Texas at Austin, Austin, TX, USA

Keywords Shale gas · Rock mechanics · Bedding plane · Single plane of weakness theory · Drilling fluid · Borehole stability

List of symbols

C_t	Compressive strength after an immersion time of t
C_0	Compressive strength before immersion
E_h	Young's modulus parallel to the bedding plane
E_v	Young's modulus normal to the bedding plane
E_{γ_a}	Young's modulus at a given angle of γ_a
G_{hh}	Shear modulus parallel to the bedding plane
G_{vh}	Shear modulus normal to the bedding plane
P_w	Mud weight
S_t	Shear strength after an immersion time of t
S_0	Shear strength before immersion
v_{hh}	Poisson's ratio parallel to the bedding plane
v_{vh}	Poisson's ratio normal to the bedding plane
β	Angle between the normal direction of the weak plane and σ_1
θ	Circumferential angle on the wellbore wall
σ	Normal stress
σ_1	Maximum principal stress
σ_3	Minimum principal stress
σ_{rr}	Radial stress around the borehole
σ_{zz}	Axial stress around the borehole
$\sigma_{\theta\theta}$	Tangential stress around the borehole
τ	Shear stress
τ_o	Cohesion of the rock matrix
τ_o'	Cohesion of the weak plane
φ	Friction angle of the rock matrix
φ'	Friction angle of the weak plane
ε	Normal strain
γ	Shear strain

γ_a Angle between the load direction and the bedding plane

1 Introduction

Shale gas is an important unconventional resource (Zou et al. 2010). The estimated shale gas reserve worldwide is 623 trillion cubic meters according to a report from the Energy Information Administration, and the shale gas will continue to play an important role in the future global energy market (Yuan et al. 2012). For economic and safe developments of shale gas, knowledge of mechanical characteristics of gas shale is important for wellbore stability analysis, well trajectory optimization, and hydraulic fracturing design (Zhao et al. 2004; Jiang 2011; Yan et al. 2013; Sone and Zoback 2013a, 2014; Guo et al. 2014; Rasouli and Sutherland 2014). It is well known that the mechanical properties of gas shale are very different from those of tight sands and carbonate rocks due to the extremely tight matrix, preexisting natural fractures, and bedding planes (Zhang et al. 2007; Liu et al. 2008; You et al. 2014). Only few laboratory test results on the mechanical characteristics of gas shale have been published compared with conventional rocks. Vernik and Nur (1992) investigated the velocity anisotropy of organic-rich black shale and concluded that the anisotropy is mainly due to the non-uniform shale microstructure. Lo et al. (1986) studied the elastic anisotropy of Chicopee shale under various confining pressures and demonstrated that the shale retains a residual anisotropy under high confining pressures due to its particularly internal particle arrangement. Niandou et al. (1997) found that the Tournemire shale displays clearly anisotropic, plastic deformation based on conventional triaxial tests and loading/unloading tests. Kuila et al. (2011) argued that shale anisotropy is induced by complex field stress environments and found that shale samples remain highly anisotropic under high confining pressures. Sone and Zoback (2013a, b, c, 2014) studied the geomechanical problems for various shale gas reservoirs in North America. They experimentally analyzed the anisotropically mechanical properties and their relationships with the velocity anisotropy of organic-rich shales. In particular, they documented creep characteristics of organic-rich shales, which had been long neglected, and analyzed the impact of shale creep on horizontal stresses.

Failure of gas shale is dependent on the properties of both the shale matrix and the bedding planes (Liang et al. 2014; Heng et al. 2015). Experimental results have shown that the strength of gas shale is a function of the angle between the axial stress and the bedding plane (Yuan et al. 2013; Fjær and Nes 2013). However, in the previous studies, the influence of drilling fluid on the mechanical properties of gas shale was not considered. Invasion of drilling fluid into the gas shale can occur while drilling. The gas shale usually contains abundant clay minerals. The time required to drill a horizontal well in shale gas is relatively long and borehole instability problems tend to occur in the late time of drilling because of drilling fluid invasion (You et al. 2014). For example, the drilling period for Well W201-H1 in the Sichuan Basin in southwest China is 72 days. The post-drilling wiper trip takes 38 days and the volume of caved shale collected at the surface is as high as 35 m^3. Therefore, understanding the influence of drilling fluid on the mechanical characteristics of gas shale is vital for solving the wellbore instability problems. In this paper, an experimental study is conducted to investigate the effects of drilling fluids on the strength of the shale matrix and bedding planes. The mechanisms for the effects of different drilling fluids are discussed.

2 Characteristics of the Gas Shale Samples

The gas shale samples used in this study were obtained from the Sichuan Basin, China. The samples were sent to the laboratory for testing as soon as possible after coring to avoid weathering and loss of water content. The measured porosities of the samples, using the helium expansion method, are 2–6%. The matrix permeability is less than 0.01 mD under the in situ stress conditions, but the local fracture-related permeability can be very high. X-ray diffraction (XRD) was used to analyze the mineral contents of the samples and the results are reported in Table 1 and Table 2. The samples consist of 28.8–47.5% quartz (38.3% in average) and 33.9–50.7% clay minerals (41.9% in average). The clay contains 37–45% illite, 36–46% mixed-layer illite/smectite (I/S), and some chlorite and kaolinite. No pure smectite is present in the samples.

The gas shale formations usually have a well-laminated structure (Fig. 1) due to the originally depositional characteristics and the continuous changes in compositions and structures of the formation under deep burial conditions (Suarez-Rivera et al. 2005). Therefore, different rock properties may exhibit along the directions parallel and normal to the laminated planes due to the organized distributions of clay minerals (Hornby 1994; Sondergeld and Rai 2011) and compliantly organic materials (Sondergeld et al. 2000; Vernik and Milovac 2011).

Scanning electron microscope (SEM) was used to study the microstructural characteristics of the gas shales and regularly oriented micro-fractures were observed, as shown in Fig. 2.

The transverse isotropy of gas shale is first exhibited in its elasticity (Hornby 1994). Many experiments have

Table 1 Mineral components of the gas shale

No.	Quartz (%)	K-feldspar (%)	Plagioclase (%)	Calcite (%)	Dolomite (%)	Pyrite (%)	Salt (%)	Clay (%)
1	35.4	0.9	1.3	4.4	4.0	6.5	–	47.5
2	47.5	–	1.9	5.9	3.7	4.3	1.3	35.4
3	37.4	1.2	1.5	4.5	4.9	16.6	–	33.9
4	28.8	–	1.9	4.9	3.7	3.2	6.8	50.7
5	42.4	–	2.1	5.2	4.7	3.5	–	42.1

Table 2 Mineral components of the clay minerals

No.	Mineral components of the clay minerals (%)						Smectite components in the mixed layer (S%)	
	Smectite	I/S[1]	Illite	Kaolin	Chlorite	C/S[2]	I/S	C/S
1	–	41	39	8	12	–	20	–
2	–	39	42	6	13	–	25	–
3	–	36	45	6	13	–	28	–
4	–	46	37	7	10	–	26	–
5	–	41	43	5	11	–	22	–

[1] I/S—mixed-layer illite/smectite

[2] C/S—mixed-layer chlorite/smectite

Fig. 1 Photograph of gas shale

shown that shale is a transverse, isotropic material (Yuan 2014) in which the elastic modulus parallel to the bedding plane is usually 10–150% greater than that perpendicular to the bedding plane. However, in the matrix between the bedding planes, very little difference is observed in different directions (Cho et al. 2012; Sayers 2013; Sone and Zoback 2014; Yuan 2014; Yan et al. 2015).

We measured the P-wave velocities of the gas shale samples under the atmospheric pressure at different directions, from parallel to perpendicular to the bedding planes with an incremental angle of 30°, as shown in Fig. 3. The Intelligent Ultrasonic Apparatus of Rock was used for the measurements. The apparatus has a sampling frequency of 10 MHz, a sensor frequency of 0.35 MHz, and a time accuracy of 0.1 μs. The P-wave measurement results are shown in Table 3.

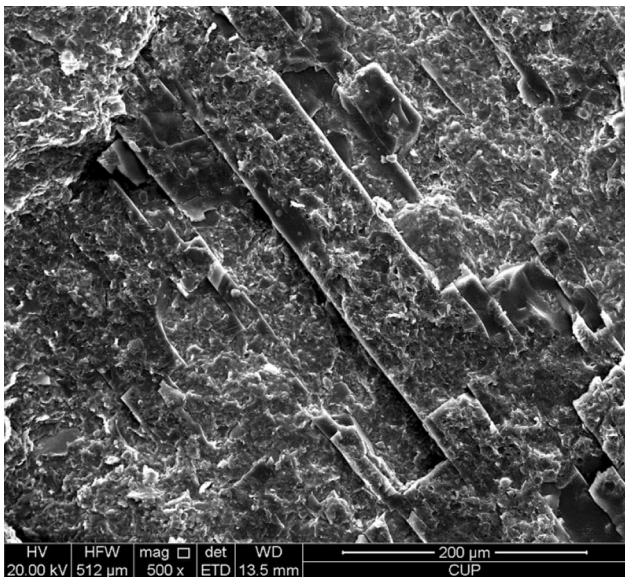

Fig. 2 Parallel micro-fractures in the gas shale

The difference in the P-wave velocities parallel to the bedding plane is small (<113 m/s), but the difference between the parallel and the perpendicular directions to the bedding plane is significantly larger, with a maximum difference of 851 m/s. The results support that gas shale can be characterized as a transversely isotropic material.

The constitutive equation of the stress–strain relationship of a transversely isotropic material can be expressed as follows (Sayers 2005):

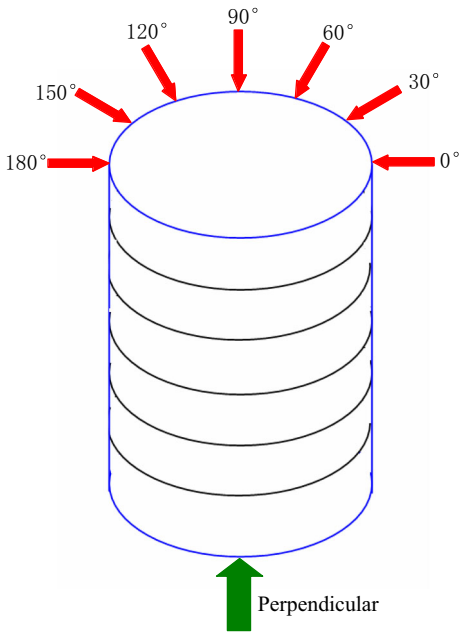

Fig. 3 P-wave velocity testing directions

Table 3 P-wave velocity results

Angle (°)	P-wave velocity (m/s)
Parallel to the bedding plane	
0	4849
30	4904
60	4937
90	4898
120	4843
150	4824
180	4849
Perpendicular to the bedding plane	4086

$$\begin{pmatrix} \varepsilon_{xx} \\ \varepsilon_{yy} \\ \varepsilon_{zz} \\ \gamma_{yz} \\ \gamma_{zx} \\ \gamma_{xy} \end{pmatrix} = \begin{pmatrix} \frac{1}{E_h} & -\frac{\nu_{hh}}{E_h} & -\frac{\nu_{vh}}{E_v} & & & \\ -\frac{\nu_{hh}}{E_h} & \frac{1}{E_h} & -\frac{\nu_{vh}}{E_v} & & & \\ -\frac{\nu_{hv}}{E_h} & -\frac{\nu_{hv}}{E_h} & \frac{1}{E_v} & & & \\ & & & \frac{1}{G_{vh}} & & \\ & & & & \frac{1}{G_{vh}} & \\ & & & & & \frac{1}{G_{hh}} \end{pmatrix} \begin{pmatrix} \sigma_{xx} \\ \sigma_{yy} \\ \sigma_{zz} \\ \tau_{yz} \\ \tau_{zx} \\ \tau_{xy} \end{pmatrix} \tag{1}$$

where σ and τ are the normal and shear stress components, respectively; ε and γ are the normal and shear strain components, respectively; E_v and E_h are the Young's modulus normal and parallel to the bedding plane, respectively; ν_{vh} and ν_{hv} are the Poisson's ratio parallel and normal to the bedding plane, respectively, due to the imposed vertical strain; ν_{hh} is the Poisson's ratio parallel to the bedding plane due to the imposed parallel strain; G_{hh} and G_{vh} are the shear modulus parallel and normal to the bedding plane, respectively.

Considering the isotropy in the direction parallel to the bedding, the shear modulus G_{hh} can be expressed as a function of E_h and ν_{hh}:

$$G_{hh} = \frac{E_h}{2(1+\nu_{hh})} \tag{2}$$

The mechanical property matrix for elastic materials in Eq. 1 must be symmetric to satisfy thermodynamic requirements (Gautam and Wong 2006). Therefore, the following equation should hold:

$$\frac{\nu_{hv}}{E_h} = \frac{\nu_{vh}}{E_v} \tag{3}$$

Among the seven elasticity parameters in Eq. 1, only five are independent. These five parameters, E_v, E_h, ν_{vh}, ν_{hh} and G_{vh}, can fully describe transversely isotropic materials, as shown in Eq. 4.

$$\begin{pmatrix} \varepsilon_{xx} \\ \varepsilon_{yy} \\ \varepsilon_{zz} \\ \gamma_{yz} \\ \gamma_{zx} \\ \gamma_{xy} \end{pmatrix} = \begin{pmatrix} \frac{1}{E_h} & -\frac{\nu_{hh}}{E_h} & -\frac{\nu_{vh}}{E_v} & & & \\ -\frac{\nu_{hh}}{E_h} & \frac{1}{E_h} & -\frac{\nu_{vh}}{E_v} & & & \\ -\frac{\nu_{vh}}{E_v} & -\frac{\nu_{vh}}{E_v} & \frac{1}{E_v} & & & \\ & & & \frac{1}{G_{vh}} & & \\ & & & & \frac{1}{G_{vh}} & \\ & & & & & \frac{2(1+\nu_{hh})}{E_h} \end{pmatrix} \begin{pmatrix} \sigma_{xx} \\ \sigma_{yy} \\ \sigma_{zz} \\ \tau_{yz} \\ \tau_{zx} \\ \tau_{xy} \end{pmatrix} \tag{4}$$

These five independent elasticity parameters can be determined using laboratory tests (Sarout et al. 2007). We measured the static elasticity parameters of the gas shale as follows: E_v and ν_{vh} were measured via a uniaxial compressive test on a core sample with its axis normal to the bedding plane. E_h and ν_{hh} were measured via a uniaxial compressive test on a sample with its axis parallel to the bedding plane. In addition to these uniaxial compressive tests, core samples with their axes intersecting the bedding plane at angles other than 0° and 90° (in this case, 45°) were used to determine G_{vh}. The elastic modulus was calculated as follows (Cho et al. 2012; Wang et al. 2012):

$$\frac{1}{E_{\gamma_a}} = \frac{\sin^4\gamma_a}{E_h} + \left(\frac{1}{G_{vh}} - 2\frac{\nu_{vh}}{E_v}\right)\cdot \sin^2\gamma_a \cos^2\gamma_a + \frac{\cos^4\gamma_a}{E_v} \tag{5}$$

where γ_a is the angle between the load direction and the bedding plane; E_{γ_a} represents Young's modulus measured at a given γ_a.

Based on the test results, the five independent elasticity parameters of the transversely isotropic shale were calculated using Eq. (5) and the results are shown in Table 4. These results were obtained by averaging the measurements of several groups of uniaxial compressive tests. For the tests in the same loading direction, the measurement results are very similar, with the largest relative difference <10%.

3 Experimental Methods

The transverse isotropy of gas shales exhibits not only in their elastic properties but also in the strength, which is greatly influenced by the weak bedding planes (Chenevert 1964; Higgins et al. 2008). To study the failure of such rocks, several failure criteria for anisotropic rocks have been proposed (Jaeger 1960; Walsh and Brace 1964; Gol'denblat and Kopnov 1965; Mclamore and Gray 1967; Karr et al. 1989; Hill 1998; Tien and Kuo 2001; Mortara 2010). However, these criteria usually involve many parameters which require a large number of core tests to determine. For gas shale, it is usually difficult and expensive to obtain enough cores. Therefore, selecting a simple and practical failure criterion suitable for gas shale is important. The single plane of weakness theory proposed by Jaeger (1960) is a concise and widely used strength criterion for anisotropic rocks, which requires relatively less and easy-to-determine parameters.

The single plane of weakness theory assumes that the layered rock has two failure modes: shear failure along the bedding plane and shear failure of the rock matrix. The failure criterion for the rock matrix is expressed by Eq. 6.

$$\tau = \tau_o + \sigma \tan \varphi \tag{6}$$

where σ is the normal stress on the failure plane; τ is the shear stress on the failure plane; τ_o and φ are the cohesion and the friction angle of the rock matrix, respectively. Through this paper, compressive stress is taken as positive.

The failure criterion for the weak plane is defined as:

$$\tau = \tau_o' + \sigma \tan \varphi' \tag{7}$$

where σ and τ are the normal stress and shear stress on the weak plane, respectively; τ_o' and φ' are the cohesion and friction angle of the weak plane, respectively.

When transforming the stresses on a matrix failure plane and on a weak bedding plane into principal stresses σ_1 and σ_3, Eqs. 6 and 7 become Eqs. 8 and 9, respectively.

Table 4 Summary of the anisotropic parameters of the shale

E_v (GPa)	E_h (GPa)	v_{vh}	v_{hh}	G_{vh} (GPa)
20	24	0.18	0.21	18

$$(\sigma_1 - \sigma_3) = \frac{2(\tau_0 + \sigma_3 \tan \varphi)}{\sqrt{\tan^2 \varphi + 1} - \tan \varphi} \tag{8}$$

$$(\sigma_1 - \sigma_3) = \frac{2(\tau_o' + \sigma_3 \tan \varphi')}{(1 - \tan \varphi' \mathrm{cotan}\beta) \sin 2\beta} \tag{9}$$

where β is the angle between the normal direction of the weak plane and σ_1. For values of β approaching 90° or in the range of 0° to φ', slip on the plane of weakness cannot occur.

Because the strength of gas shale is jointly controlled by the matrix strength and bedding plane strength, the impacts of drilling fluid on both of them were tested. Two groups of standard core samples (ϕ25 mm × 50 mm) were drilled using a diamond coring bit with kerosene as the cooling medium. Abrasive papers were used to smooth the end surfaces of the shale samples until the roughness is less than ±0.05 mm. The axes of the samples are perpendicular to both end surfaces with a discrepancy less than ±0.25°. One group of the samples with the axis normal to the bedding plane was used to study the matrix strength using conventional triaxial tests. The other group with the axis parallel to the bedding plane was used to measure the bedding plane strength using direct shear tests. Because the acoustic wave velocities are related to the rock mechanical properties, acoustic wave velocity tests were also conducted under the same conditions and only samples with similar wave velocities in each group were selected for the strength tests. The wave velocities of the samples perpendicular to the bedding plane range from 4075 to 4113 m/s, while the velocities parallel to the bedding plane are between 4845 and 4869 m/s. The similar wave velocities imply that the core samples have similar mechanical parameters in the corresponding directions.

The selected samples were then immersed in water-based mud (WBM) and oil-based mud (OBM) at a temperature of 60 °C. To investigate the influence of immersion time on shale strength, the samples were immersed for various durations, i.e., 1, 2, 4, 6, 8, and 10 days. To prevent the drilling fluid from evaporating from the immersed shale samples, strength tests were carried out immediately after the samples were taken out from the drilling fluid.

It should be noted that the use of kerosene as the cooling liquid while coring the samples may influence water absorption when the samples are immersed in WBM because the kerosene may change the wettability of the core surface and increase the resistance to water infiltration. Consequently, the estimated impact of the WBM may be smaller in the experiments than in the real situations. To mitigate this effect, the kerosene on the sample surface was wiped off using oil-absorbing papers immediately after coring and then the samples were placed in an oven, drying for 24 h at a temperature of 60 °C before immersing them in WBM. This should have effectively removed the

residual kerosene on the samples and eliminated its influence on the strength tests.

When the axial stress of a sample is normal to the bedding plane in a triaxial compressive test, shear failure along the bedding plane is unlikely to occur. Instead, the failure plane will cross the bedding plane as illustrated in Fig. 4. To determine the cohesion and friction angle of the shale matrix after immersing the samples for a certain time, two tests, at least, are required to conduct on two cores with the same immersion time but under different confining pressures. These tests were carried out using the MTS Rock Test System (Fig. 5). During the loading process, a constant axial displacement rate of 1 μm/s was used to control the increase in the axial load. The displacement gauge can measure displacements up to 5 mm with a resolution of ±1 μm.

The strength of shale bedding planes is measured using the direct shear tests. The device used for the direct shear tests was modified from an existing equipment in the rock mechanics laboratory at China University of Petroleum and the schematic diagram of the device is shown in Fig. 6. During the tests, a normal load was applied to a preset value using the load-control method. And then, a constant shear displacement rate of 0.3 mm/min was used to apply the shear load until the failure of the sample while keeping the normal stress constant. Because no available extra servo-controlled system was available at the time of the experiments, a hand pump was used to apply the normal load for all the tests. This is a deficiency of the tests because the subjectivity may impact the test results. However, the hand pump was only used to apply the normal load, which should only have limited effects on the test results. The shear load was applied using a servo-controlled system for all the tests.

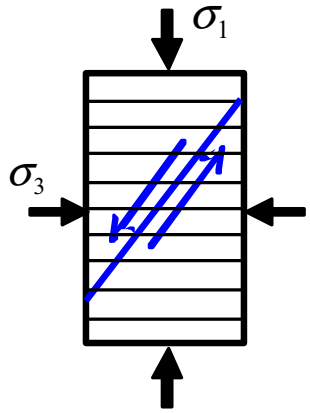

Fig. 4 Failure mode in the triaxial compressive test

Fig. 5 MTS Rock Test System

To determine the cohesion and the friction angle of the bedding plane after immersion in the drilling fluid, two cores at least with the same immersion time also need to be tested. Assuming that the normal stresses acting on the bedding plane are σ_{n1} and σ_{n2} in the two tests and the measured shear strengths of the bedding plane are τ_1 and τ_2, respectively, the cohesion and friction angle of the bedding plane can be determined as follows:

$$\left.\begin{aligned} \varphi' &= \tan^{-1}\left(\frac{\tau_2 - \tau_1}{\sigma_{n2} - \sigma_{n1}}\right) \\ \tau_o' &= \tau_1 - \sigma_{n1}\tan\varphi' \end{aligned}\right\}. \tag{10}$$

4 Shear Strength Test Results

4.1 Impacts of Drilling Fluid on Shale Matrix Strength

In this study, 13 pairs of triaxial tests were conducted, including one group without immersion,six pairs with WBM immersion,and six pairs with OBM immersion. The test results are summarized in Table 5. Based on the Mohr's theory of strength, the test results are plotted in the normal-shear stress plane and the failure envelopes for different immersion times with WBM and OBM are obtained, as shown in Figs. 7 and 8, respectively. The results show that the failure envelopes move down (shear failure occurs at a lower shear stress) after immersion in the drilling fluid, indicating the strength of shale matrix gradually decreases. The changes of compressive strengths with immersion time for different drilling fluids and confining pressures are shown in Fig. 9.

The shale matrix strength decreases after immersion in both WBM and OBM. However, the impact of WBM is much larger than that of OBM. After an immersion time of

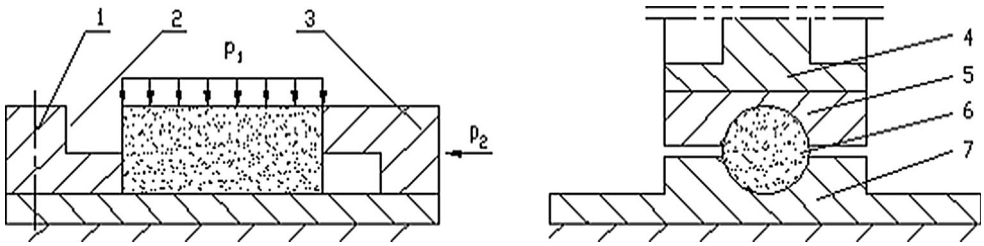

Fig. 6 Diagram of direct shear testing equipment. *1* Positioning bolt hole, *2* immobile indenter, *3* mobile indenter, *4* piston connected with handheld pump, *5* mobile indenter connected to the jack, *6* core sample, *7* baseboard

Table 5 Shale matrix strength

Immersion time (days)	WBM				OBM			
	Failure strength (MPa)		Cohesion (MPa)	Friction angle (°)	Failure strength (MPa)		Cohesion (MPa)	Friction angle (°)
	Confining pressure of 0 MPa	Confining pressure of 20 MPa			Confining pressure of 0 MPa	Confining pressure of 20 MPa		
0	91.30	156.93	25.22	32.24				
1	88.21	152.51	24.61	31.68	90.20	155.29	25.03	31.97
2	84.66	147.39	23.95	31.12	88.75	153.31	24.67	31.8
4	72.03	129.22	21.28	28.81	85.54	148.53	24.14	31.22
6	65.72	120.25	19.93	27.63	83.44	145.41	23.66	30.81
8	64.27	118.58	19.47	27.55	82.92	144.64	23.61	30.66
10	63.49	117.59	19.31	27.43	82.75	144.22	23.58	30.59

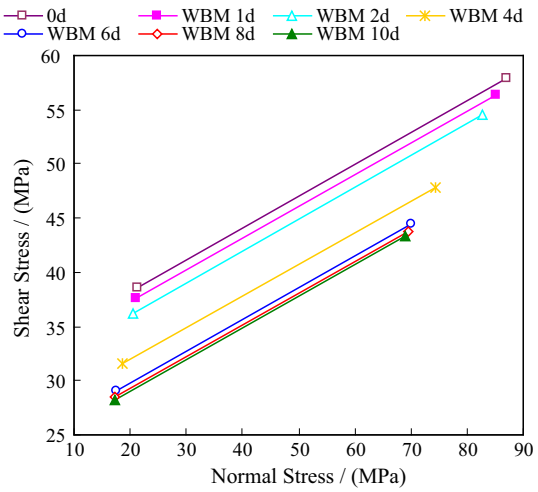

Fig. 7 Shale matrix strength in the normal-shear stress plane (immersed in WBM)

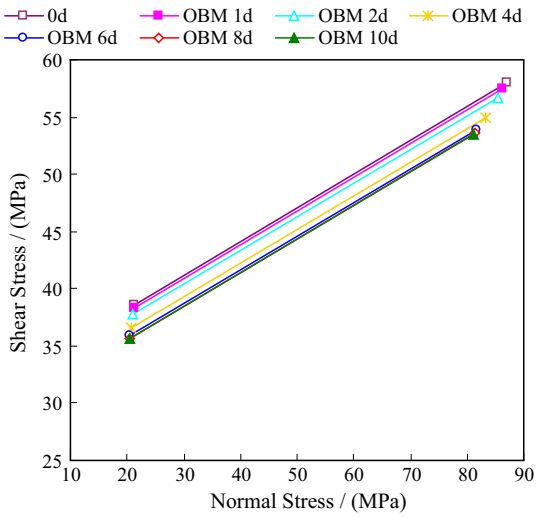

Fig. 8 Shale matrix strength in the normal-shear stress plane (immersed in OBM)

10 days, the uniaxial compressive strength of the shale matrix decreases by 30 and 9% in WBM and OBM, respectively. Nevertheless, the time-dependent patterns of shale matrix strength with immersion time for both WBM and OBM are similar, which can be divided into an initial slow-decreasing stage, a following rapid-decreasing stage, and a final stable stage.

4.2 Impacts of Drilling Fluid on Bedding Plane Strength

The direct shear strengths of the samples with their axes parallel to the bedding plane for different immersion times were tested and the results are reported in Table 6. The normal-shear stress failure envelopes of the bedding plane

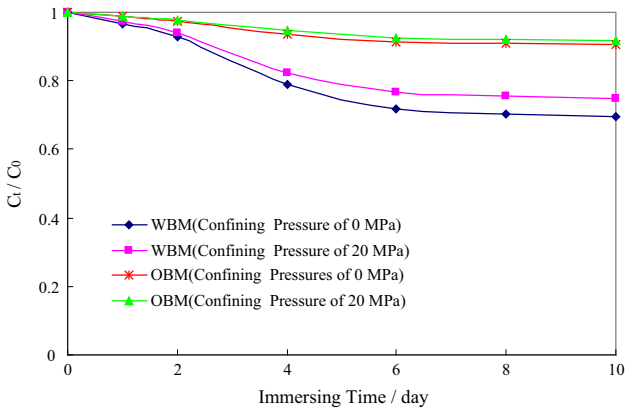

Fig. 9 Compressive strength of the shale matrix versus immersion time (C_t represents the compressive strength with an immersion time of "*t*," C_0 represents the compressive strength before immersion)

for different immersion times with WBM and OBM are shown in Figs. 10 and 11, respectively. Similar to the shale matrix, the failure envelopes of the bedding plane move down after immersion in drilling fluid, indicating the shear strength of the bedding plane decreases gradually. The relationships between the bedding plane shear strength and the immersion time are shown in Fig. 12.

Figure 12 shows that the immersion in drilling fluid significantly reduces the shear strength of the bedding plane. The impact of WBM is much larger compared with OBM. The shear strength of the bedding plane under a normal stress of 5 MPa after 10 days of immersion in WBM decreases by 79% (5.78 MPa). If no countermeasures are taken in the drilling operations, this strength reduction can cause catastrophic results. However, in OBM, only a decrease of 28% in shear strength was observed under the same condition. Both the cohesion and the friction angle of the bedding plane decreases with the increase of immersion time.

The test results also show that, regardless of whether the samples are immersed in WBM or OBM, the impact of drilling fluids on the bedding plane strength is always greater than on the shale matrix strength.

5 Interpretations and Discussions

The changes of the cohesion and friction angle of the bedding plane with immersion time are different from those of the shale matrix. No initial slowly decreasing stage of the shear strength is observed. Instead, the strength decrease is rapid at the beginning of immersion and then slows down gradually. Finally, the shear strength reaches a stable value, as shown in Fig. 12. Because the bedding planes usually have relatively high permeability compared with shale matrix (McLellan and Cormier 1996; Yu et al. 2007; Yan et al. 2014a), the drilling fluid will first seep into the bedding planes while drilling, resulting in the hydration of the clay minerals in the bedding planes and lowering bedding strength. Conversely, the permeability and water sensitivity of the shale matrix are much lower, so it exhibits strength decrease only after being in contact with the drilling fluid for a relatively long time.

Intergranular fractures and micro-cracks are common in gas shale. The bedding planes are usually cemented with filling materials, as shown in Fig. 13. The cementation is usually loose and fragile. When the shale comes into contact with drilling fluid, the fluid will invade into the shale through the intergranular micro-fractures and micro-cracks (Fig. 14), driven by physicochemical effects such as chemical potential and capillary pressure (Guo 2013). The filtrate invasion affects the bedding plane mainly in two ways: (1) increasing the fluid pressure inside the micro-fractures and, accordingly, reducing the effective normal stress on the fracture plane (Jaeger et al. 2007) and (2)

Table 6 Shear strength of the bedding plane

Immersion time (days)	WBM				OBM			
	Shear strength (MPa)		Cohesion (MPa)	Friction angle (°)	Shear strength (MPa)		Cohesion (MPa)	Friction angle (°)
	Normal stress of 5 MPa	Normal Stress of 15 MPa			Normal stress of 5 MPa	Normal stress of 15 MPa		
0	7.34	12.20	4.91	25.9				
1	6.25	10.58	4.08	23.4	6.84	11.54	4.48	25.2
2	5.18	8.84	3.35	20.1	6.44	11.09	4.12	24.9
4	2.99	5.64	1.67	14.8	5.75	10.12	3.56	23.6
6	2.02	4.07	0.99	11.6	5.30	9.45	3.23	22.5
8	1.67	3.58	0.72	10.8	5.16	9.27	3.11	22.3
10	1.56	3.45	0.61	10.7	4.92	8.99	2.89	22.1

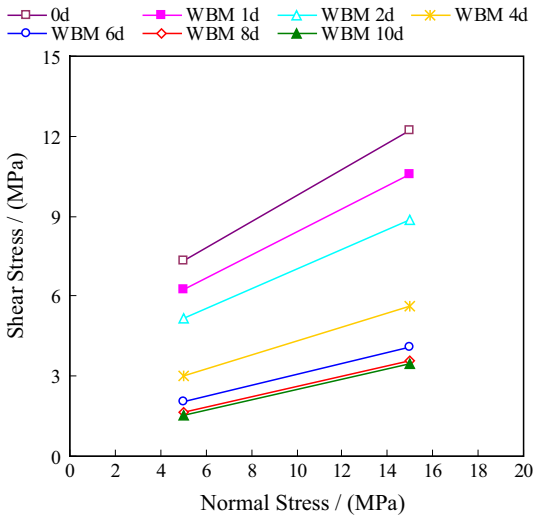

Fig. 10 Bedding plane strength in the normal-shear stress plane (immersed in WBM)

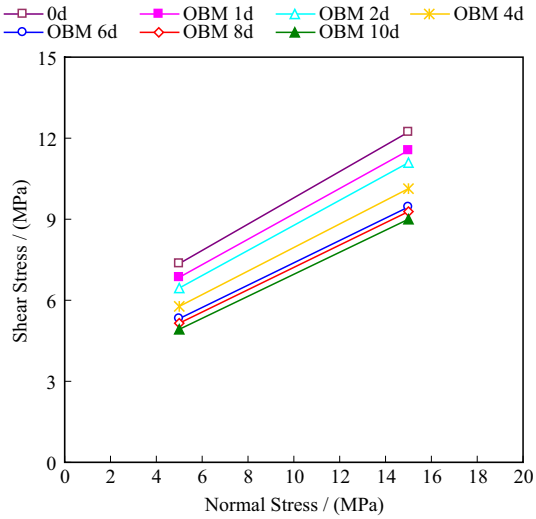

Fig. 11 Bedding plane strength in the normal-shear stress plane (immersed in OBM)

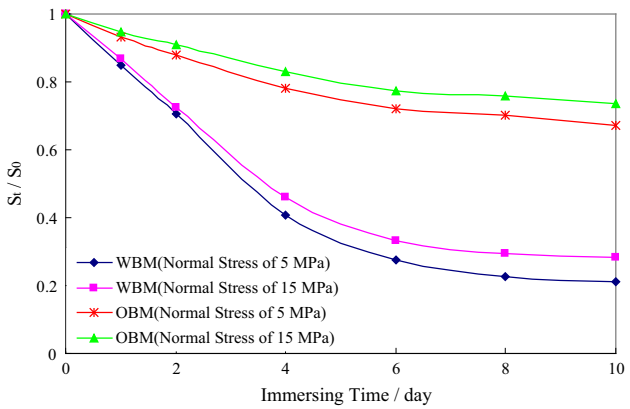

Fig. 12 Shear strength of the bedding plane versus immersion time (S_t represents the shear strength with an immersion time of "t," S_0 represents the shear strength before immersion)

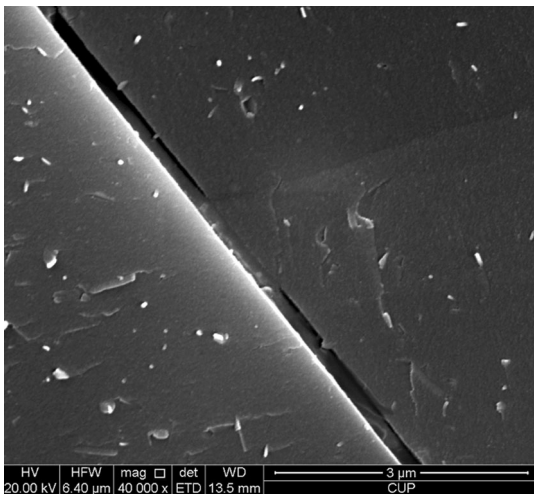

Fig. 13 Cementation of a micro-fracture

Fig. 14 Capillary self-absorbing phenomenon of shale

altering the properties of the internal fracture planes in the shale. When in contact with drilling fluid, the water-sensitive shale will absorb water, resulting in a chemical reaction as shown in Eq. 11 (Yang et al. 2006). This reaction can lubricate the fracture plane (Yan et al. 2014a) and reduce the friction inside the fracture. This will accelerate the propagation of the micro-cracks due to the increased stress transmission to the crack tip and the ultimate decrease in the strength of the fracture plane. Meanwhile, different forms of water present in shale, including solid water, water vapor, bound water, adsorbed water, gravitational water (free water), and capillary water, as shown in Fig. 15. The drilling fluids may diffuse into the

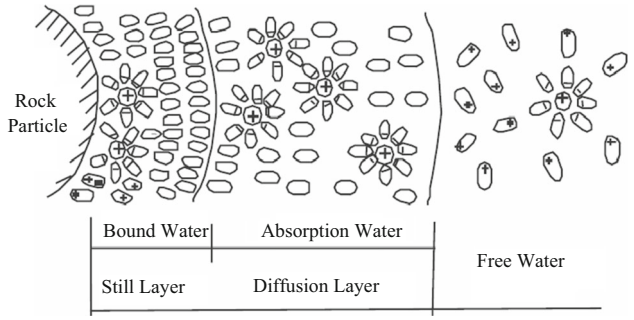

Fig. 15 Water states in shale

shale due to physical and/or chemical driving forces. Drilling fluid diffusion will lead to increases in the amount of the absorbed water and in the thickness of the diffusion layer around the rock particles. As a result, the shale volume will increase and swelling stress will be induced. The swelling stress of the shale particles may reduce the strength of the shale and facilitate the growth of the microcracks.

$$\begin{aligned} &K_{0.9}Al_{2.9}Si_{3.1}O_{10}(OH)_2{+}nH_2O \\ &\quad\rightarrow K_{0.9}Al_{2.9}Si_{3.1}O_{10}(OH)_2nH_2O \end{aligned} \tag{11}$$

The molecules of polar water can interact with the hydroxyls on the surfaces of the mineral particles, replacing the hydrogen bond between the particles (Hadizadeh and Law 1991) and hydrating the contact point between the particles. This process can lead to erosion, dissolution, or shrinkage of the mineral particles. Consequently, the cohesion between particles may decrease or disappear, causing hydration-driven disintegration and dispersion (Shi et al. 2012). Moreover, as mentioned above, the hydration of the bedding plane cementations improves the lubrication. The increase in water content can cause a significant effect due to the water–membrane bonding between the bedding plane particles, and then the frictional contact becomes a water–membrane contact which decreases the intergranular friction effect (Liu and Li 2012). Therefore, the Mohr circles of the bedding plane strength move to the left in the normal-shear stress plane after the sample is immersed in drilling fluid. Mechanically, the lubricating effect of water on the bedding plane decreases its friction angle. Therefore, the samples tend to fail along the preexisting micro-fractures after being immersed in a WBM. However, OBMs have less impact on the bedding plane properties due to their weak polarity.

In shale matrix, the extremely low permeability and the lack of water-sensitive minerals result in chemical inertness between the drilling fluid and the matrix, so hydration rarely occurs. The strength of the shale matrix is less affected by the drilling fluid than the bedding plane strength. When the fluid filtrate becomes saturated in the rock, the shale stops absorbing water and the shale strength reaches a steady value.

In field operations, the speed of drilling fluid invasion can be more rapid than that in laboratory experiments due to the large pressure difference between the formation and the wellbore. Thus, the decrease rate of shale strength may be larger than that observed in the experiments. However, the strength of gas shale will ultimately reach a stable value due to the lack of water-sensitive minerals. Because the drilling fluid mainly affects the weak bedding planes, which is more prone to fail while drilling compared with shale matrix, the appropriate use of plugging materials in the drilling operations can minimize fluid invasion into the bedding planes. This technique can effectively reduce the hydration and erosion of the bedding plane cementations, thereby improving the long-term stability of the wellbores while drilling in gas shale formations.

6 Field Application: Borehole Stability Analysis

The development of shale gas generally requires the use of horizontal or highly inclined wells. The stress around a borehole in an anisotropic formation includes two parts: the far field stress before drilling and the boundary stress induced by anisotropy during drilling (Aadnoy 1987; Ong 1994). Based on the concepts of generalized plane strain and linearly elasticity, the stress distribution around a wellbore in a transversely isotropic formation can be described as:

$$\left.\begin{aligned} \sigma_{xx} &= \sigma_{xx,0} + 2\mathrm{Re}\left[\mu_1^2\phi_1'(z_1) + \mu_2^2\phi_2'(z_2)\right] \\ \sigma_{yy} &= \sigma_{yy,0} + 2\mathrm{Re}\left[\phi_1'(z_1) + \phi_2'(z_2)\right] \\ \tau_{xy} &= \tau_{xy,0} - 2\mathrm{Re}\left[\mu_1\phi_1'(z_1) + \mu_2\phi_2'(z_2)\right] \\ \tau_{xz} &= \tau_{xz,0} + 2\mathrm{Re}\left[\mu_3\phi_3'(z_3)\right] \\ \tau_{yz} &= \tau_{yz,0} - 2\mathrm{Re}\left[\phi_3'(z_3)\right] \\ \sigma_{zz} &= \sigma_{zz,0} - \frac{1}{a_{33}}\left(a_{31}\sigma_{xx,a} + a_{32}\sigma_{yy,a}\right) \end{aligned}\right\} \tag{12}$$

where

$$\left.\begin{aligned} \phi_1'(z_1) &= \frac{1}{2\Delta(\mu_1\cos\theta - \sin\theta)} \times (E'\mu_2 - D') \\ \phi_2'(z_2) &= \frac{1}{2\Delta(\mu_2\cos\theta - \sin\theta)} \times (D' - E'\mu_1) \\ \phi_3'(z_3) &= \frac{1}{2\Delta(\mu_3\cos\theta - \sin\theta)} \times (F'\mu_2 - \mu_1) \end{aligned}\right\} \tag{13}$$

$$\left.\begin{aligned} \Delta &= \mu_2 - \mu_1 \\ D' &= \left(P_w - \sigma_{xx,0}\right)\cos\theta - \tau_{xy,0}\sin\theta - i\left(P_w - \sigma_{xx,0}\right) \\ &\quad \sin\theta - i\tau_{xy,0}\cos\theta \\ E' &= -\left(P_w - \sigma_{yy,0}\right)\sin\theta + \tau_{xy,0}\cos\theta - i\left(P_w - \sigma_{yy,0}\right) \\ &\quad \cos\theta - i\tau_{xy,0}\sin\theta \\ F' &= -\tau_{xz,0}\cos\theta - \tau_{yz,0}\sin\theta + i\tau_{xz,0}\sin\theta - i\tau_{yz,0}\cos\theta \end{aligned}\right\} \tag{14}$$

where σ_{xx} , σ_{yy} , σ_{zz} , τ_{xy} , τ_{xz} ,and τ_{yz} are the stress components around the wellbore in a rectangular coordinate system; the stress components with the subscripts of "0" and "a" are far field stresses before drilling and the boundary stresses induced by anisotropy during drilling, respectively; θ is the circumferential angle on the wellbore wall; Re is the notation for the real part of the complex expressions in the brackets; a_{31}, a_{32}, and a_{33} are the components of the compliance coefficient matrix of the material $\phi(z_k)\,(k = 1, 2, 3)$ represents the analytic functions of the complex variable $z_k = x + \mu_k y$; μ_k is the characteristic root of the characteristic equation corresponding to the strain compatibility equation; P_w is the mud pressure acting on the borehole wall.

The above equations are established in a rectangular coordinate system, but it is more convenient to conduct borehole stability analysis using a borehole cylindrical coordinate system (Chen et al. 2008; Yan et al. 2014b). Therefore, the stresses in Eq. 12 are converted to a cylindrical coordinate system as follows:

$$\begin{pmatrix} \sigma_{rr} \\ \sigma_{\theta\theta} \\ \sigma_{zz} \\ \tau_{\theta z} \\ \tau_{rz} \\ \tau_{r\theta} \end{pmatrix} = \begin{bmatrix} \cos^2\theta & \sin^2\theta & 0 & 0 & 0 & 2\sin\theta\cos\theta \\ \sin^2\theta & \cos^2\theta & 0 & 0 & 0 & -2\sin\theta\cos\theta \\ 0 & 0 & 1 & 0 & 0 & 0 \\ 0 & 0 & 0 & \cos\theta & -\sin\theta & 0 \\ 0 & 0 & 0 & \sin\theta & \cos\theta & 0 \\ -\sin\theta\cos\theta & \sin\theta\cos\theta & 0 & 0 & 0 & \cos^2\theta - \sin^2\theta \end{bmatrix} \begin{pmatrix} \sigma_{xx} \\ \sigma_{yy} \\ \sigma_{zz} \\ \tau_{yz} \\ \tau_{xz} \\ \tau_{xy} \end{pmatrix} \tag{15}$$

where σ_{rr},$\sigma_{\theta\theta}$ and σ_{zz} are the radial, tangential, and axial stress around the wellbore, respectively; $\tau_{\theta z}$, τ_{rz} and $\tau_{r\theta}$ are shear stresses.

The maximum principal stress σ_1 and minimum principal stress σ_3 on the wellbore wall can be determined as (Fjar et al. 2008; Zhu et al. 2015):

$$\left.\begin{aligned} \sigma_1 &= \frac{(\sigma_{\theta\theta} + \sigma_{zz})}{2} + \sqrt{\left(\frac{\sigma_{\theta\theta} - \sigma_{zz}}{2}\right)^2 + \tau_{\theta z}^2} \\ \sigma_3 &= \sigma_{rr} \end{aligned}\right\} \tag{16}$$

In bedding shales, borehole failure may include two modes: shale matrix failure and bedding plane failure (Zhang 2013). The single plane of weakness theory is used to describe the failure of shale in this paper: matrix failure and bedding plane failure are defined by Eqs. 8 and 9, respectively (Jaeger 1960).

The collapse pressure is the minimum wellbore pressure required to maintain wellbore stability while drilling. The collapse pressure of a well in a gas shale formation can be determined by inserting Eq. 16 into the single plane of weakness theory Eqs. 8 and 9. Furthermore, the time-dependent collapse pressure due to drilling fluid invasion can be evaluated by combining the testing results in Sect. 4.

For determining the time-dependent collapse pressure, elastic parameters shown in Table 4 were used. The shale formation is under an overburden pressure of 62 MPa, a maximum horizontal stress of 52.3 MPa, and a minimum horizontal stress of 43.5 MPa. The formation pressure is 26 MPa. These values were obtained through an inversion method based on the leak-off test results. The direction of maximum horizontal stress is N90°E. The bedding dip of the shale formation is 30° and the dip direction is 0°. The Biot's coefficient of the formation is 0.7.

Figures 16 and 17 show the time-dependent collapse pressures for WBM and OBM, respectively. The collapse pressures increase with drilling time, but the increasing rate reduces with time and becomes very small after 6 days. The collapse pressure is nearly constant after 10 days, which can be regarded as the final collapse pressure with drilling fluid invasion. When drilling along the direction of the minimum horizontal stress, the final collapse pressure is 1.90 and 1.58 g/cm^3 for WBM and OBM, respectively. When drilling along the direction of the maximum horizontal stress, the final collapse pressure is 1.56 and 1.30 g/cm^3 for WBM and OBM, respectively.

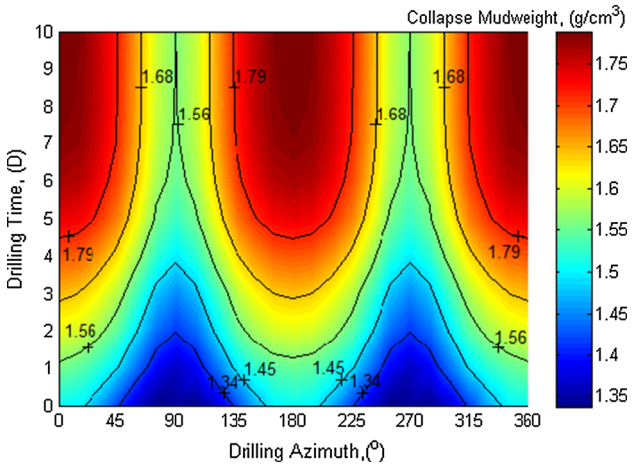

Fig. 16 Time-dependent collapse pressure with WBM

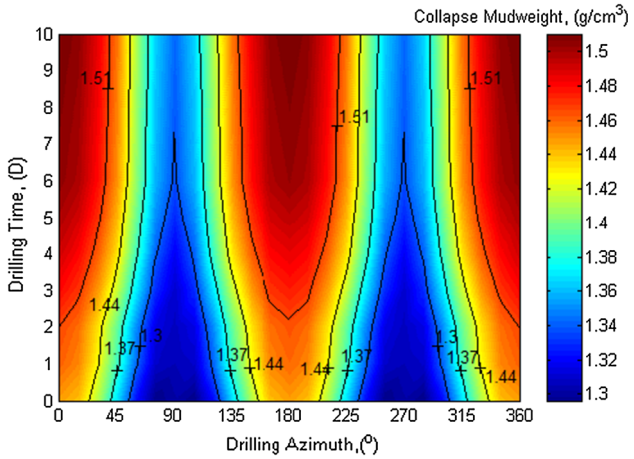

Fig. 17 Time-dependent collapse pressure with OBM

For the case drilling along minimum horizontal stress direction using WBM which requires a mud density higher than 1.90 g/cm^3 to maintain wellbore stability, the borehole pressure is very close to the minimum horizontal stress. Under this situation, fracturing of the wellbore and the resulting lost circulation can easily occur in bedding shale formations. To mitigate this problem, OBM is recommended. However, when drilling along the direction of the maximum horizontal stress, the final collapse pressure is low, even for WBM. Therefore, WBM and OBM can both satisfy the wellbore stability requirements and the engineers can have more flexibility in selecting the mud type at a rig site. From the viewpoint of avoiding wellbore instability, horizontal wells are recommended to be drilled along the direction of the maximum horizontal stress.

7 Conclusions

The gas shale is characterized by the presence of clay minerals and a laminated structure. It can be treated as a transversely isotropic material and its strength is jointly controlled by the matrix strength and the bedding plane strength.

Drilling fluid immersion significantly decreases the strength of shale matrix and bedding plane. WBM has a much greater impact on shale strength than OBM. The drilling fluid immersion has a much larger impact on the bedding plane strength than on the shale matrix strength. The changes in shale matrix strength with immersion time can be divided into an initial slow-decreasing stage, an intermediate rapid-decreasing stage, and a final stable stage. Differently, the bedding plane strength exhibits a rapid decrease from the very beginning of immersion and then slows down.

When shale comes into contact with drilling fluid, the fluid invades the rock through the intergranular microfractures and micro-cracks in the shale. The fluid invasion affects the bedding plane in two ways, i.e., increasing the fluid pressure inside the micro-fractures with the accompanying decrease in the effective normal stress on the fracture planes and altering the properties of the internal fracture planes in the shale. Conversely, the strength of the shale matrix is less affected by the drilling fluid because it usually has extremely low permeability and very little water-sensitive minerals compared to the bedding planes.

The collapse pressure gradually increases as the drilling time increases. WBM filtration results in a larger increase in collapse pressure compared with OBM. Thus, OBM is recommended for drilling bedding shale formations to maintain the long-term stability of the borehole.

Acknowledgements The authors would like to thank the editor and the anonymous reviewers for their helpful and constructive comments. This work is financially supported by the Changjiang Scholars and Innovative Research Team in University (Grant No. IRT_14R58), the National Basic Research Program of China (973 Program) (Grant No. 2015CB251201), the National Natural Science Foundation Project of China (Grant No. 51574270 and 51504280), Fundamental Research Funds for the Central Universities (Grant No. 15CX02009A), the Qingdao Science and Technology Project (Grant No. 15-9-1-55-jch).

References

Aadnoy BS (1987) Continuum mechanics analysis of the stability of inclined boreholes in anisotropic rock formations. Ph.D. Thesis. Norwegian Institute of Technology, University of Trondheim

Chen M, Jin Y, Zhang GQ (2008) Petroleum related rock mechanics. Science Press, Beijing

Chenevert ME (1964) The deformation-failure characteristics of laminated sedimentary rocks. University of Texas

Cho JW, Kim H, Jeon S, Min KB (2012) Deformation and strength anisotropy of Asan gneiss, Boryeong shale, and Yeoncheon schist. Int J Rock Mech Min Sci 50:158–169

Fjær E, Nes OM (2013) Strength anisotropy of Mancos shale. In: Proceedings of the 47th US rock mechanics/geomechanics symposium. San Francisco

Fjar E, Holt RM, Raaen AM, Risnes R, Horsrud P (2008) Petroleum related rock mechanics. Elsevier Science, Amsterdam

Gautam R, Wong RC (2006) Transversely isotropic stiffness parameters and their measurement in Colorado shale. Can Geotech J 43(12):1290–1305

Gol'denblat II, Kopnov VA (1965) Strength of glass-reinforced plastics in the complex stress state. Mech Comp Mater 1(2):54–59

Guo TK (2013) Mechanism Research on Hydraulic Fracturing by Stimulated Reservoir Volume (SRV) for Shale Play. Ph.D. Thesis. China University of Petroleum (Beijing)

Guo TK, Zhang SC, Qu ZQ, Zhou T, Xiao YS, Gao J (2014) Experimental study of hydraulic fracturing for shale by stimulated reservoir volume. Fuel 128:373–380

Hadizadeh J, Law RD (1991) Water-weakening of sandstone and quartzite deformed at various stress and strain rates. Int J Rock Mech Min Sci Geomech Abstr 28(5):431–439

Heng S, Guo Y, Yang C, Daemen JJ, Li Z (2015) Experimental and theoretical study of the anisotropic properties of shale. Int J Rock Mech Min Sci 74:58–68

Higgins S, Goodwin S, Donald A, Bratton T, Tracy G (2008) Anisotropic stress models improve completion design in the Baxter Shale. In: SPE annual technical conference and exhibition, Denver, Colorado

Hill R (1998) The mathematical theory of plasticity. Oxford University Press, Oxford

Hornby BE (1994) The elastic properties of shales. Ph.D. Thesis. University of Cambridge

Jaeger JC (1960) Shear failure of anisotropic rocks. Geol Mag 97(1):65–72

Jaeger J, Cook NGW, Zimmerman R (2007) Fundamentals of rock mechanics. Blackwell, London

Jiang S (2011) Geological theory innovations and advances in drilling and completion technology for shale gas development. Pet Drill Technol 39(3):17–23

Karr DG, Law FP, Fatt MH, Cox GF (1989) Asymptotic and quadratic failure criteria for anisotropic materials. Int J Plast 5(4):303–336

Kuila U, Dewhurst DN, Siggins AF, Raven MD (2011) Stress anisotropy and velocity anisotropy in low porosity shale. Tectonophysics 503(1):34–44

Liang C, Chen M, Jin Y, Lu Y (2014) Wellbore stability model for shale gas reservoir considering the coupling of multi-weakness planes and porous flow. J Nat Gas Sci Eng 21:364–378

Liu J, Li JP (2012) Study of shear strength water sensitivity of intact schist from Guzhu expressway. Rock Soil Mech 33(6):1719–1723

Liu RH, Feng WG, Long L (2008) Experimental studies on the mechanics and acoustics of tight carbonate rock. Pet Geol Oilfield Dev Daqing 27(6):131–134

Lo T, Coyner KB, Toksöz MN (1986) Experimental determination of elastic anisotropy of Berea sandstone, Chicopee shale, and Chelmsford granite. Geophysics 51(1):164–171

McLamore R, Gray KE (1967) The mechanical behavior of anisotropic sedimentary rocks. J Eng Ind 89:62

McLellan PJ, Cormier K (1996) Borehole instability in fissile, dipping shales, Northeastern British Columbia. In: SPE gas technology symposium. Alberta

Mortara G (2010) A yield criterion for isotropic and cross-anisotropic cohesive-frictional materials. Int J Numer Anal Methods Geomech 34(9):953–977

Niandou H, Shao JF, Henry JP, Fourmaintraux D (1997) Laboratory investigation of the mechanical behaviour of Tournemire shale. Int J Rock Mech Min Sci 34(1):3–16

Ong SH (1994) Borehole stability. Ph.D. Thesis. University of Oklahoma

Rasouli V, Sutherland A (2014) Geomechanical characteristics of gas shales: a case study in the North Perth Basin. Rock Mech Rock Eng 47(6):2031–2046

Sarout J, Molez L, Guéguen Y, Hoteit N (2007) Shale dynamic properties and anisotropy under triaxial loading: experimental and theoretical investigations. Phys Chem Earth 32(8):896–906

Sayers CM (2005) Seismic anisotropy of shales. Geophys Prospect 53(5):667–676

Sayers CM (2013) The effect of anisotropy on the Young's moduli and Poisson's ratios of shales. Geophys Prospect 61(2):416–426

Shi B, Xia B, Lin Y (2012) CT imaging and mechanism analysis of crack development by hydration in hard-brittle shale formations. Act Pet Sin 33(1):137–142

Sondergeld, CH, Rai CS, Margesson RW, Whidden KJ (2000) Ultrasonic measurement of anisotropy on the Kimmeridge shale. In: 70th annual international meeting, SEG. Alberta

Sondergeld CH, Rai CS (2011) Lead Edge 30(3):324–331

Sone H, Zoback M (2013a) Relation between creep compliance and elastic modulus in organic-rich shales observed through laboratory experiments. In: EGU general assembly conference abstracts. Vienna

Sone H, Zoback MD (2013b) Mechanical properties of shale-gas reservoir rocks—part 1: static and dynamic elastic properties and anisotropy. Geophysics 78(5):381–392

Sone H, Zoback MD (2013c) Mechanical properties of shale-gas reservoir rocks—part 2: ductile creep, brittle strength, and their relation to the elastic modulus. Geophysics 78(5):393–402

Sone H, Zoback MD (2014) Time-dependent deformation of shale gas reservoir rocks and its long-term effect on the in situ state of stress. Int J Rock Mech Min Sci 69:120–132

Suarez-Rivera R, Green S, Handwerger D, Martin W, Kieschnick J (2005) Accounting for heterogeneity provides a new perspective for completions in tight gas shales. In: The 40th US symposium on rock mechanics (USRMS). Alaska

Tien YM, Kuo MC (2001) A failure criterion for transversely isotropic rocks. Int J Rock Mech Min Sci 38(3):399–412

Vernik L, Milovac J (2011) Rock physics of organic shales. Lead Edge 30(3):318–323

Vernik L, Nur A (1992) Ultrasonic velocity and anisotropy of hydrocarbon source rocks. Geophysics 57(5):727–735

Walsh JB, Brace WF (1964) A fracture criterion for brittle anisotropic rock. J Geophys Res 69(16):3449–3456

Wang Q, Wang P, Xiang DG, Feng YS (2012) Anisotropic property of mechanical parameters of shales. Nat Gas Ind 32(12):62–65

Yan C, Deng JG, Yu B, Tan Q, Deng FC, Zhu H, Hu L, Chen Z (2013) Research on collapsing pressure of gas shale. Chin J Rock Mech Eng 32(8):1595–1602

Yan C, Deng J, Yu B, Liu H, Deng F, Chen Z, Hu L, Zhu H, Han Q (2014a) Wellbore stability analysis and its application in the Fergana basin, central Asia. J Geophys Eng 11(1):1–9

Yan C, Deng J, Yu B, Li W, Chen Z, Hu L, Li Y (2014b) Borehole stability in high-temperature formations. Rock Mech Rock Eng 47(6):2199–2209

Yan C, Deng J, Hu L, Chen Z, Yan X, Lin H, Tan Q, Yu B (2015) Brittle failure of shale under uniaxial compression. Arab J Geosci 8(5):2467–2475

Yang C, Mao H, Wang X, Li X, Chen J (2006) Study on variation of microstructure and mechanical properties of water-weakening slates. Rock Soil Mech 27(12):2090–2098

You L, Kang Y, Chen Z (2014) Wellbore instability in shale gas wells drilled by oil-based fluids. Int J Rock Mech Min Sci 72:294–299

Yu BH, Deng JG, Wang HG (2007) Borehole stability technique for Huoerguosi anticline, Junggar Basin, North west China. Pet Explor Dev 34(1):108–112

Yuan JL (2014) Mechanical properties evaluation of shale reservoir and engineering applications. Ph.D. Thesis. China University of Petroleum (Beijing)

Yuan J, Deng J, Yu B, Tan Q, Fan B (2012) Wellbore stability of horizontal wells in shale gas reservoirs. Nat Gas Ind 32(9):66–70

Yuan JL, Deng JG, Tan Q, Yu BH, Jin XC (2013) Borehole stability analysis of horizontal drilling in shale gas reservoirs. Rock Mech Rock Eng 46(5):1157–1164

Zhang J (2013) Borehole stability analysis accounting for anisotropies in drilling to weak bedding planes. Int J Rock Mech Min Sci 60:160–170

Zhang H, Kang Y, Cheng J (2007) Experimental study on mechanical properties of dense sandstone under different confining pressures. Chin J Rock Mech Eng 26(S):4227–4231

Zhao JZ, LI ZK, Sun JJ, Yan J, Dong GH, Li R (2004) Triaxial stress test of rock and primary research on the rule of compaction effect. J Univ Pet 28(4):56–58

Zhu H, Deng J, Jin X, Hu L, Luo B (2015) Hydraulic fracture initiation and propagation from wellbore with oriented perforation. Rock Mech Rock Eng 8(2):585–601

Zou C, Dong D, Wang S, Li J, Li X, Wang Y, Cheng K (2010) Geological characteristics and resource potential of shale gas in China. Pet Explor Dev 37(6):641–653